Cirrhosis-associated liver nodules in Egyptian patients: correlation of histopathologic and MRI with diffusion findings

Lamiaa I.A. Metwally[a], Sanaa A.M. El Tatawy[a], Naglaa A.H. Zayed[b]

[a]Department of Radiology, Faculty of Medicine, [b]Department of Endemic Medicine and Hepatology, Faculty of Medicine, Cairo University, Egypt

Correspondence to Lamiaa I.A. Metwally, MD, Assistant Professor, Department of Radiology, Faculty of Medicine, Cairo University, Kasr Al Ainy hospital, Al-Saray St., El Manial, Cairo, 11956, Egypt. Tel: 23634717; e-mail: lili2973@yahoo.com

Received 18 March 2019
Accepted 10 July 2019

Kasr Al Ainy Medical Journal 2019, 25:7–21

Aim
This study aimed to examine the role of enhanced MRI combined with diffusion in the characterization of cirrhotic nodules, to differentiate benign cirrhotic nodules from premalignant and malignant ones, and to determine treatment planning and management.
Patients and methods
Precontrast T1, T2, T2-Spectral Attenuated Inversion Recovery, in-phase and out-phase gradient echo sequence, dynamic contrast-enhanced, and diffusion-weighted MRI, *b* values (0, 500, 1000 s/mm) were obtained in 40 patients with cirrhotic liver (total of 58 focal nodules). The morphological features of each lesion were recorded: size, shape, margin, signal, pattern of contrast enhancement, number, and site of focal lesions in the diffusion images with apparent diffusion coefficient values.
Results
Lesions were divided according to MR diagnosis and divided histopathologically into four groups: group A: malignant, group B: premalignant (dysplastic), group C: regeneration, and group D: siderotic nodules. Histopathologically, they were divided into 26 hepatocellular carcinoma, nine low-grade dysplastic, nine high-grade dysplastic, 12 regeneration, and two siderotic nodules. The accuracy of MRI was 93%, the sensitivity was 100%, and the specificity was 70% in this study.
Conclusion
Contrast-enhanced MRI with diffusion-weighted imaging is sensitive for early detection of malignant neoplastic hepatic lesions, and for differentiation between premalignant and malignant lesions.

Keywords:
cirrhosis, diffusion-weighted imaging, liver, MRI, nodules

Kasr Al Ainy Med J 25:7–21

1687-4625

Introduction

Cirrhotic liver is characterized by irreversible remodeling of the hepatic architecture with bridging fibrosis and a broad range of hepatocellular nodules. The common causes of cirrhosis include hepatitis C virus (55% of cases), hepatitis B virus (16%), and alcohol consumption (13%), and other causes are cryptogenic nonalcoholic fatty liver disease and nonalcoholic steatohepatitis (16%) [1,2].

Imaging surveillance in high-risk patients with cirrhosis for development of hepatocellular carcinoma (HCC) is crucial. According to the American Association for the Study of Liver Diseases (AASLD) and the European Association for the Study of the Liver European Organization for Research and Treatment of Cancer guidelines, HCC nodules are diagnosed if larger than 10 mm and if they show characteristic MRI post-contrast arterial uptake and washout in venous phases [3].

In 1995, guidelines for the classification and description of nodular hepatocellular lesions were published by an International Working Party panel. According to these guidelines, nodular hepatocellular lesions were classified as follows: regenerative nodules, dysplastic nodules, HCC, and siderotic nodules [4–6].

MRI is considered an important modality for the diagnosis of cirrhosis and its complications. It aids characterization, follow-up of the increase in size, vascularity of nodules, and detection of gradual carcinogenesis [2,7].

The diffusion-weighted technique is used as an additional sequence to supplement conventional MR protocol studies. Along with measurement of its

 DOI: 10.4103/kamj.kamj_9_19

apparent diffusion coefficient (ADC), both enable proper characterization of hepatic lesions [8,9].

The aim of our work is to study the role of enhanced MRI combined with diffusion in the characterization of cirrhotic nodules, to differentiate benign cirrhotic nodules from premalignant and malignant ones, and to determine treatment planning and management.

Patients and methods

Patients

The study was approved by the hospital's ethical committee, and an informed consent was obtained assuring respect of the confidentiality of the medical data and information. The study design was observational analytical. Forty (24 men and 16 women) patients were enrolled over a period of 6 months. The patients included were cases known to have cirrhotic liver with focal hepatic nodules detected by ultrasound (US) and/or multi-slice computed tomography (MSCT). They were referred from the Outpatient Clinics and Inpatient Departments at Kasr Al-Ainy University Hospital and the National Cancer Institute. All of them were HCV positive. We excluded cases with cirrhotic liver with no hepatic nodules and patients with acute renal insufficiency to avoid hepatorenal syndrome with an IV gadolinium-diethylene–triamine–penta-acetic acid (Gd-DTPA) injection.

The patients were subjected to the following:

(1) Full clinical assessment including recording of age, sex, and clinical presentation.
(2) Laboratory investigations: liver biochemical profile, alanine transaminase, aspartate aminotransferase, α-fetoprotein, and renal function tests.
(3) Abdominal MRI [precontrast and postcontrast study and diffusion-weighted imaging (DWI)].
(4) Biopsy and histopathological analysis were carried out for the suspicious focal lesions on US and/or MSCT, and the results of the previously obtained biopsies for some patients were also included in the study.

Methods

All patients underwent an MRI examination of the abdomen. Twenty-five out of the 40 patients underwent both US and MSCT before MR examination, whereas the remaining 15 patients underwent only US.

MRI

All the patients underwent MRI on high-field system (1.5 Tesla) magnet units (Philips Intera, Philips Gyroscan Intera (Philips Healthcare, Amsterdam, Netherlands)) using a phased array coil to cover the whole liver. Conventional MRI, post Gd-DTPA dynamic, and diffusion MRI studies were obtained. First, the detection and characterization of focal lesions were performed on conventional precontrast and dynamic contrast-enhanced images; second, the diffusion images with ADC values were reviewed.

MRI protocol

(1) Precontrast images:
Conventional precontrast images included T1-weighted images (T1WIs), T2-weighted images (T2WIs), T2-Spectral Attenuated Inversion Recovery (SPAIR) images, and in-phase and out-phase gradient echo images (GRE). The images were obtained in axial and coronal planes using the parameters listed in Table 1.
(2) Dynamic contrast-enhanced images:
A dynamic study was performed after a bolus injection of 0.1 mmol/kg body weight of Gd-DTPA at a rate of 2 ml/s, flushed with 20 ml of a sterile 0.9% saline solution through the antecubital vein. The injection of contrast medium and saline solution was performed manually. Dynamic imaging using the T1 THRIVE (high-resolution isotropic volume examination) technique was performed in a triphasic manner [arterial phase (16–20 s), porto-

Table 1 Conventional precontrast MRI parameters

	TR (ms)	TE (ms)	Matrix	Slice thickness (mm)	Slice gap (mm)	FOV (mm)
T1WI	10	4.58	179×320	7–8	1–2	355
T2WI	≥445	26–28	180–200×240	7–8	1–2	365
T2 SPAIR	≥400	80	204×384	7–8	1–2	365
In-phase and out-phase (GRE) sequence (dual/FFE)	75–100	4.6 for in-phase and 2.3 for out-phase	143×240	7–8	0	

FOV, field of view; GRE, gradient echo images; SPAIR, Spectral Attenuated Inversion Recovery; T1WIs, T1-weighted images; T2WIs, T2-weighted images; TE, echo time; TR, repetition time.

venous phase (45–60 s) and a delayed equilibrium phase (3–5 min)] after administration of the contrast medium. In some cases, we added postprocessing image subtraction for the precontrast and postcontrast axial images to evaluate the true contrast uptake in the postcontrast image of the lesions appearing with high signal intensity in the precontrast image.

(3) DWIs:
Respiratory-triggered fat-suppressed single-shot echoplanar DWI was performed in the axial plane with tri-directional diffusion gradients using *b* values (0, 500 and 1000 s/mm^2) to increase sensitivity to cellular packing. Parallel imaging with generalized auto-calibrating partially parallel acquisition using an acceleration factor of two was applied to improve image quality. The other parameters were as follows: repetition time of at least 1880 ms, echo time=70 ms, number of excitations=3, matrix 256×256, slice thickness 7–8 mm, slice gap 1–2 mm, and scan time 3–4 min with 52% rectangular field of view.

ADC calculation: The mean ADC value of each detected focal lesion was measured by sketching a region of interest over the lesion. The ADC was measured twice and the two measurements were averaged. To ensure that the same areas were measured, regions of interest were copied and pasted from DWIs to ADC maps.

MRI interpretation and analysis

The morphological features of each lesion were recorded including the size, shape, margin, signal characteristics, and pattern of contrast enhancement in the dynamic imaging as well as the number and site of the detected focal lesions. Then, a provisional diagnosis was reported. Second, we reviewed the diffusion images with ADC mapping for the different *b* values. Accordingly, the hepatic focal lesions were classified into. Thus, the patients were divided according to their MR diagnosis into four groups: group A: malignant nodules, group B: premalignant (dysplastic) nodules, group C: regeneration nodules, and group D: siderotic nodules. MRI was considered true positive when truly predicted malignant and premalignant focal lesions were proven by histopathology. The results were compared with laboratory and histopathology results in all patients and the diagnostic accuracy, sensitivity, and specificity of MRI were calculated.

Histopathological reference standard

In 1995, sets of guidelines for classification and a description of nodular hepatocellular lesions were published by an International Working Party panel. According to these guidelines, they were classified as follows:

Regenerative nodules

They may be monoacinar or multiacinar, micronodules (<3 mm), or macronodules (≥3 mm). Rarely, giant regenerative nodules (5 cm in diameter) were reported [4].

Dysplastic nodules

These are not histologically malignant or invasive and are described as either dysplastic foci (<1 mm in diameter) or dysplastic nodules (≥1 mm in diameter). According to the degree of dysplasia, these are classified as low-grade or high-grade dysplastic nodules. AASLD, stated that they should not be malignant lesions [5].

Hepatocellular carcinoma

These are composed of dedifferentiated hepatocytes. These are either small (<2 cm in diameter) or large (≥2 cm in diameter). The classic system of macroscopic classification in use since 1901 includes nodular, massive, and diffuse [4].

Siderotic nodules

This term was adopted by radiologists to describe cirrhosis-associated nodules with high levels of iron content, but histologically, they may be regenerative or dysplastic, and no imaging finding can differentiate between them; hence, the term siderotic nodule is now used [6].

Results

This study included 40 patients, 24 (60%) men and 16 (40%) women, ranging in age between 43 and 68 years, mean age 57.75 years. The total number of the primary hepatic focal lesions was 58.

The MR signal, enhancement patterns, and diffusion images criteria of the different scanned hepatic focal lesions are shown in Tables 2 and 3.

According to the histopathological results, hepatic focal lesions were categorized into four major groups (HCC, high-grade dysplastic nodules, low-grade dysplastic nodules, regeneration nodules, and siderotic nodules) (Table 4). The HCC lesions were subcategorized into well-differentiated HCC, hypovascular HCC, fat-containing HCC, HCC with necrosis, and complicated HCC with vascular invasion.

The MR signal nature, enhancement pattern, and diffusion criteria as reported in our study are listed

in Table 5 for the hepatic focal lesions studied corresponding to their histopathological category.

Group A malignant HCC nodule subcategories showed the following imaging criteria:

(1) Well-differentiated HCC (11 patients): hypointense signal on T1WI, typically hyperintense on T2 and SPAIR, restricted bright on DWIs, and low on ADC. These were hypervascular in the arterial phase of injection, with characteristic washout in portal and delayed phases with or without delayed capsular enhancement.
(2) Hypovascular HCC (two patients):
The same MR findings as those in the well-differentiated HCC, but in the dynamic study, they show no contrast uptake in all phases (i.e. remained hypointense), especially in the arterial phase (Fig. 1).
(3) Fat-containing HCC (three patients):
These were bright on T1WIs and showed signal drop in the T1W GRE out-phase compared with its high signal intensity in the T1W GRE in-phase sequences (Fig. 2).
(4) HCC with necrosis (four patients):
The necrotic areas had a bright signal on unenhanced T2WI and a low signal on T1WI, with little or no early enhancement on post-contrast images.
(5) Complicated HCC with vascular invasion (two patients):
The same MR findings as seen in the well-differentiated HCC, but associated with malignant vascular thrombus that was in close proximity to the primary tumor, characteristically expanded the involved vessel, and showed similar imaging features as the primary tumor on T1, T2WIs, and postcontrast study (Fig. 3).
Group B low-grade and high-grade dysplastic nodules (Figs 4 and 5).
Group C regeneration nodules (Fig. 6).
Group D siderotic nodules (Fig. 7).

There was a mismatch between the MR provisional diagnosis and the histopathological results in four focal lesions. According to MRI, they showed the same findings as regeneration nodules; however, they were hyperintense on T1WIs and hypointense on T2 and SPAIR WIs. There was no signal drop in the opposed-phase images compared with the in-phase images, indicating no intracellular fat content within the nodules, and were not restricted on DWIs. Accordingly, they were diagnosed as low-grade dysplastic nodules, whereas histopathological results showed them to be regeneration ones. Hence, the accuracy of MRI was 93.1%, the sensitivity was 100%, and the specificity was 70% in our study (Fig. 8).

Table 2 Precontrast MR signal pattern and diffusion nature of different hepatic focal lesions

Signal intensity	T1WIs	T2 and SPAIR WIs	Out phase	In phase	DWI and ADC map
Hypointense	23	28	5	21	
Hyperintense	25	22	9	25	
Isointense to hyperintense		4			
Isointense	10	4	44	12	
Restricted					22
Partially restricted					4
Not restricted					32

ADC, apparent diffusion coefficient; DWI, diffusion-weighted imaging; SPAIR, Spectral Attenuated Inversion Recovery; T1WIs, T1-weighted images; T2WIs, T2-weighted images.

Table 3 Enhancement pattern of different hepatic focal lesions on dynamic contrast-enhanced images

Enhancement pattern	Arterial phase	Early portal phase	Late portal phase	Delayed phase
Intense	18	9	9	9
Heterogeneous	6	3		
Minimal	7			
No contrast uptake	27	25	25	4
Washout		21	24	24
No washout				21

Discussion

MRI is an important imaging modality for the diagnosis of cirrhosis and its complications.

Table 4 Categories of hepatic focal lesions, as defined by histopathology results

	N=58	Percentage	Number of patients	Size range (cm)	Child–Pugh classification	α-Fetoprotein (ng/ml)
Hepatocellular carcinoma	26	44.82	22	2–7.3	Child A: 6Child B: 16	43–2000
Dysplastic						
High grade	9	31	15	2–4	Child A: 10Child B: 5	13–54
Low grade	9					
Regeneration	12	20.68		2–3	Child A	15–25
Siderotic	2	3.44		2–2.5	Child B	35

Table 5 MR signal, enhancement pattern, and diffusion criteria for the studied hepatic focal lesions corresponding to their histopathological category

	Hepatocellular carcinoma	Dysplastic	Regeneration	Siderotic
N	26	18	12	2
T1WIs				
Hypo	21			2
Iso			10	
Hyper	5	18	2	
T2 and SPAIR				
Hypo		18	8	2
Iso	4		4	
Hyper	22			
Out phase				
Hypo	5			Signal drop
Iso	21	9	12	
Hyper		9		
In-phase				
Hypo	21			Signal drop
Iso			10	
Hyper	5	18	2	
Diffusion-weighted imaging				
Restricted	22			
Partial restricted	4			
Not restricted		18	12	2
Dynamic study	Variable	High grade: subtle arterial enhancement, (one of them showed no arterial enhancement)Low grade: isointense in all phases	Isointense to liver in all phases, no washout	No enhancement

SPAIR, Spectral Attenuated Inversion Recovery; T1WIs, T1-weighted images; T2WIs, T2-weighted images.

Nowadays, faster sequences enable better-quality liver imaging with high intrinsic soft-tissue contrast. The dynamic contrast-enhanced studies have become a routine part of abdominal imaging; the high cost/benefit ratio and possible side effects of contrast media remain a problem [10].

In our study, the majority of group A HCC lesions were characteristically (well-differentiated HCC) hypointense on T1WIs and hyperintense on T2WIs and SPAIR, which was also noted by Gaurav *et al*. [11] and Glenn *et al*. [12] (Fig. 2). Few cases were hyperintense on T1WIs similar to the findings obtained by Rieko *et al*. [13]. This high T1 signal was related to the fat content within the lesions, where the dual out-phase and in-phase imaging technique has been valuable in the detection of intracellular fat within these nodular lesions (Fig. 1).

Few cases had iso to high signals, with a predominantly isointense signal on T2WI, and it was reported by Van *et al*. [14] in their study that the lesions may be isointense or even hypointense relative to surrounding liver on Fat Sat T2WIs.

The characteristic imaging features of HCC, including increased arterial contrast uptake and washout in the delayed phase of injection, provide very high specificity and good sensitivity in the characterization of even very small nodules. Limitations exist in the detection of hypovascular HCCs and differentiation of high-grade dysplastic nodules from early HCCs [15].

In our dynamic study, the majority of group A HCC lesions showed the typical early arterial enhancement and contrast washout in the portal and delayed phases with persistent delayed enhancing periphery "capsule". Only one case displayed no contrast uptake in the arterial phase and in the other subsequent phases (Fig. 3). These findings were also similar to those reported in the studies of Robert *et al*. [4], Jonathon *et al*. [16], and Gaurav *et al*. [11].

The combined use of conventional contrast-enhanced MRI and DWI can increase the diagnostic accuracy of MRI. DWI is a widely accepted technique and very important in the detection and differentiation of benign and malignant lesions as well as for follow-up after treatment of hepatic tumors [17,18].

Figure 1

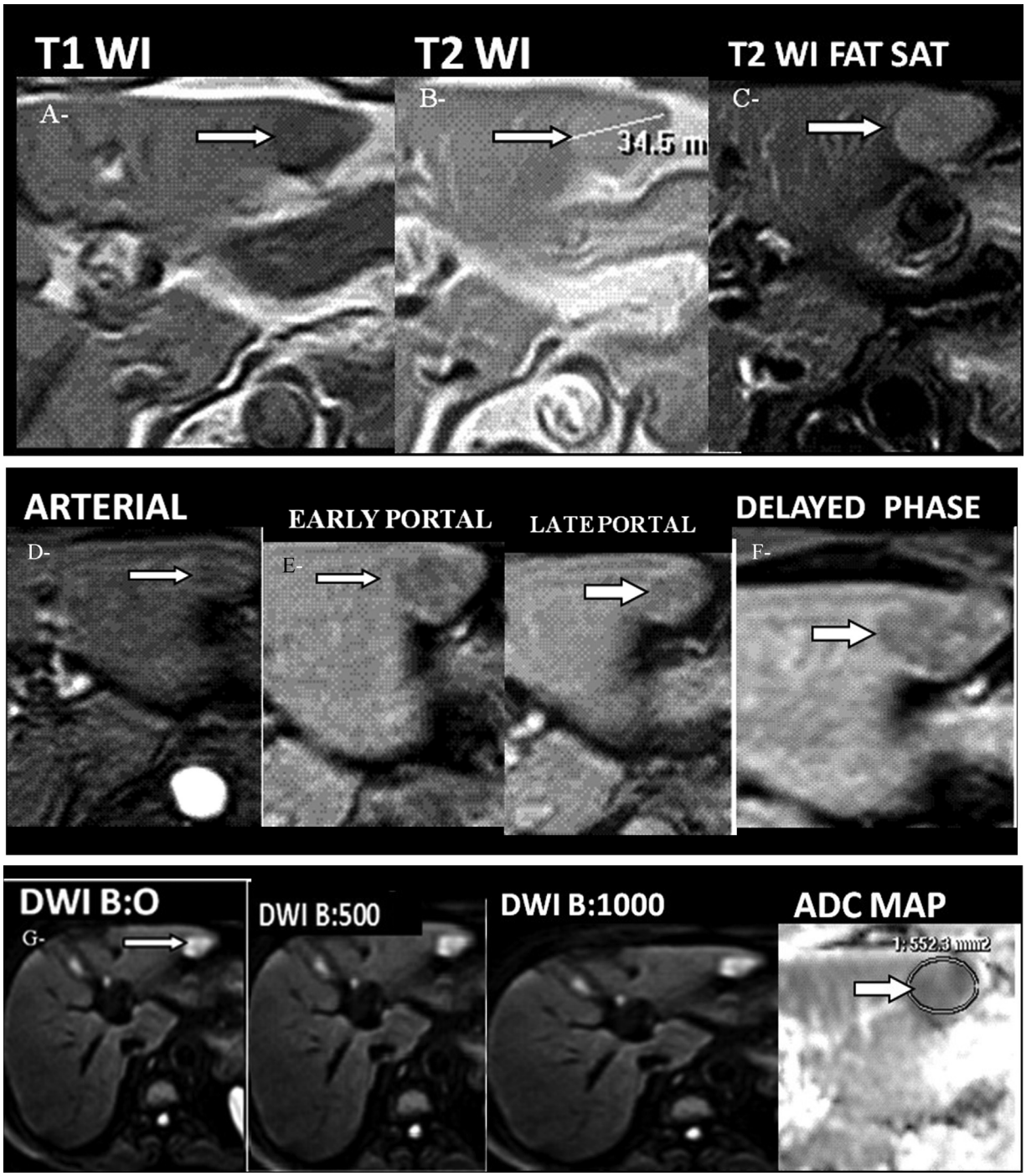

(a–g): A 68-year-old male patient presenting with right hypochondrial pain. US: Cirrhotic liver with a hypoechoic left hepatic lobe focal lesion. Laboratory investigations: α-fetoprotein: 78 ng/ml, alanine transaminase: 23, aspartate aminotransferase: 37. MRI: hypovascular hepatocellular carcinoma that was proven by histopathology. (a) Axial unenhanced T1-weighted images: a lesion of low signal intensity in the left hepatic lobe (arrow). (b) Axial T2-weighted images (T2WI): It was of mildly increased signal intensity (arrow). (c) Axial T2 fat sat image: It was of increased signal intensity (arrow). (d) Axial-enhanced arterial-phase image: no lesional contrast uptake (arrow). (e, f) Axial early and late portal as well as delayed gadolinium-enhanced images: still remaining hypointense to the liver with faint capsular enhancement in the delayed phase (arrow). (g) Diffusion-weighted imaging (DWI) (*b* 0, 500, 1000): It was of high signal intensity owing to restricted diffusion. Axial apparent diffusion coefficient map: the lesion (arrow) was of low signal intensity, proving that the high signal intensity on DWI was not T2 shine-through effect, but a truly restricted diffusion.

Our study was carried out with high *b* values (500 and 1000 s/mm^2) for DWIs to overcome the effect of capillary perfusion and water diffusion in the extracellular extravascular space as a high *b* value will result in a decrease in the signal from moving protons in the bile ducts, cysts, blood vessels, and fluid in the intestine, causing an increased contrast between the lesion and the liver. Furthermore, the differences in the

Figure 2

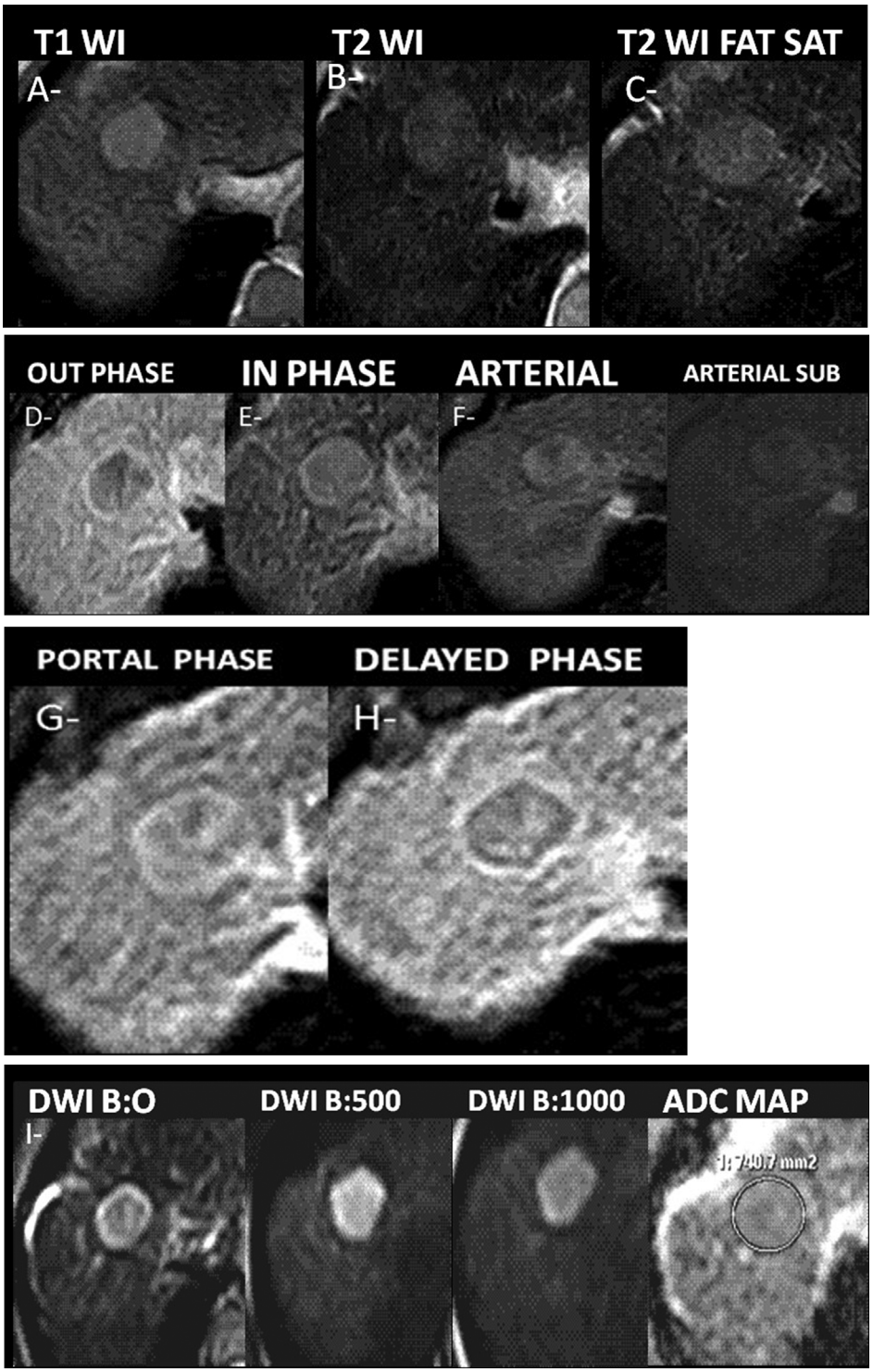

(a–i) A 63-year-old male patient presenting with right hypochondrial pain and yellowish discoloration of the sclera. US: cirrhotic liver with a hyperechoic right hepatic focal lesion. Laboratory investigations: α-fetoprotein: 76 ng/ml, alanine transaminase: 65, aspartate aminotransferase: 54. MRI: Fat containing hepatocellular carcinoma (HCC). Histopathology: Well-differentiated HCC with fat cells. (a) Axial unenhanced T1-weighted images: a lesion of high signal intensity within the right hepatic lobe. (b, c) Axial T2-weighted images (T2WI) and axial T2 fat sat: a lesion of mildly increased signal intensity. (d, e) Axial out-phase and in-phase images: signal drop of the lesion in the out-phase compared with the in-phase. (f) Axial-enhanced arterial-phase image: mild enhancement of the lesion (in the arterial subtraction image). (g, h) Axial portal and delayed enhanced images: washout of the lesion with capsular enhancement. (i) Diffusion-weighted imaging (DWI) (*b* 0, 500, 1000): the lesion had increased signal intensity owing to restricted diffusion. Axial apparent diffusion coefficient map: a lesion of mildly decreased signal intensity; hence, the high signal intensity on DWI was not T2 shine-through effect, but a truly restricted diffusion.

relative contrast ratio between malignant and benign lesions were increased with a high *b* value. This was analogous to the *b* value in the studies carried out by Demir *et al*. [19] and Hosny [10].

Figure 3

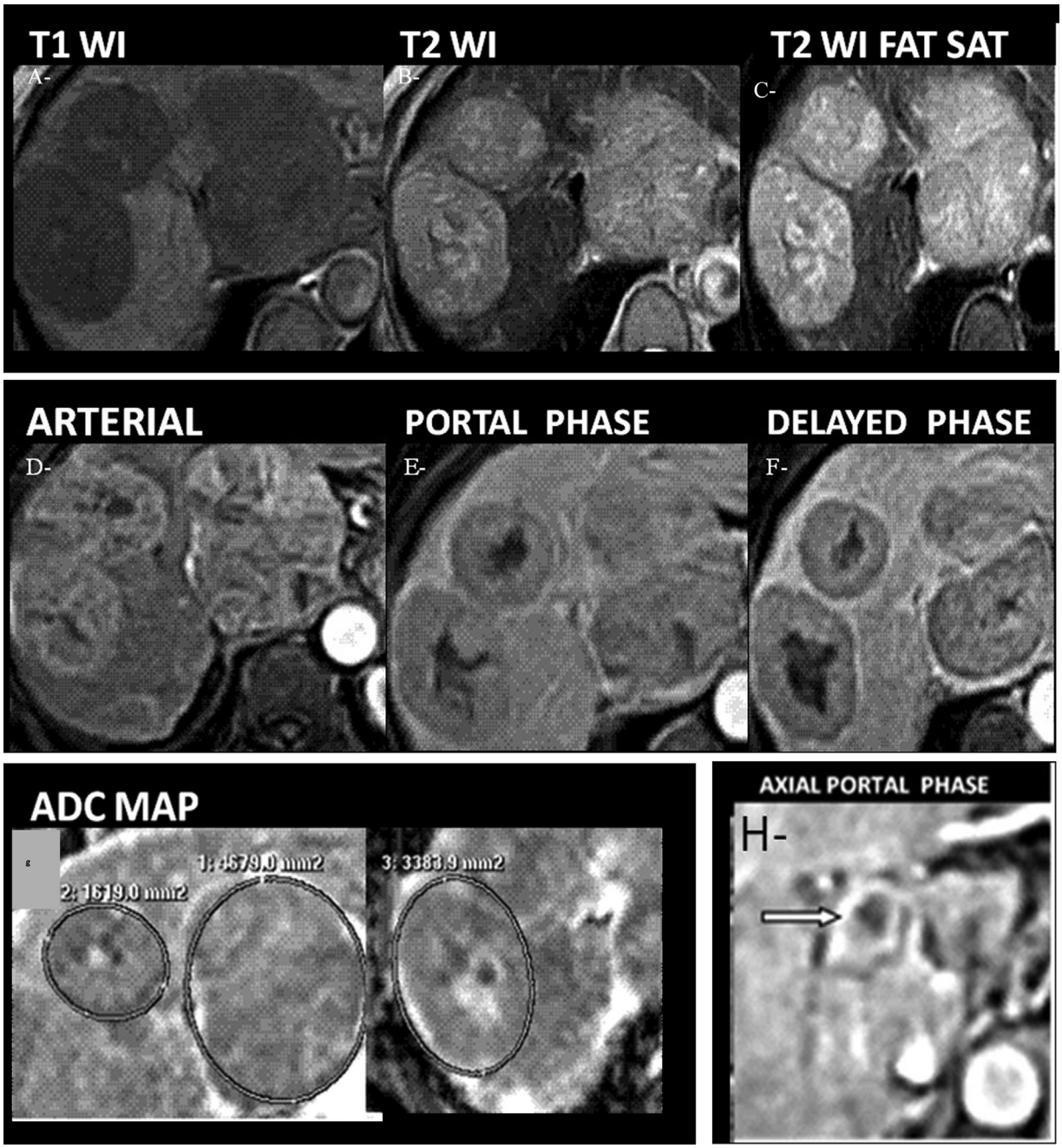

(a–h) A 60-year-old female patient presenting with hematemesis. US: Cirrhotic liver with multiple focal lesions were detected. Laboratory investigations: α-fetoprotein: 90 ng/ml, alanine transaminase: 34, aspartate aminotransferase: 53. MRI: typical hepatocellular carcinoma with portal vein thrombosis. Histopathology: Well-differentiated hepatocellular carcinoma. (a) Axial-unenhanced T1-weighted images: large three hepatic focal lesions of low signal intensity. (b. c) Axial T2-weighted images (T2WI) and T2 fat sat images: the lesions had increased signal intensity, with greater brightness in their central part. (d) Axial-enhanced arterial-phase: heterogeneously enhanced lesions with central areas of no contrast uptake (necrosis). (e, f) Axial portal and delayed enhanced images: washout of the lesions with capsular enhancement. (g) Diffusion-weighted imaging (DWI) (*b* 0, 500, 1000): they had increased signal intensity owing to restricted diffusion. Axial apparent diffusion coefficient map: they had decreased signal intensity, proving that the high signal intensity on DWI was not T2 shine-through effect, but a truly restricted diffusion. (h) Axial portal enhanced image: the portal vein was partially obliterated by a filling defect.

The majority of group A HCC lesions in our study showed restricted diffusion, and a few cases were partially restricted. These data were also reported by Gaurav *et al*. [11], who found that a mass in the cirrhotic liver with restricted diffusion favors the diagnosis of HCC.

Our work showed that few lesions of group A HCC showed a mosaic appearance on unenhanced and contrast-enhanced T1WI and T2WI, with an average diameter of 4.75 cm. This indicates that the mosaic pattern is usually observed in a large tumor. This feature was also

Figure 4

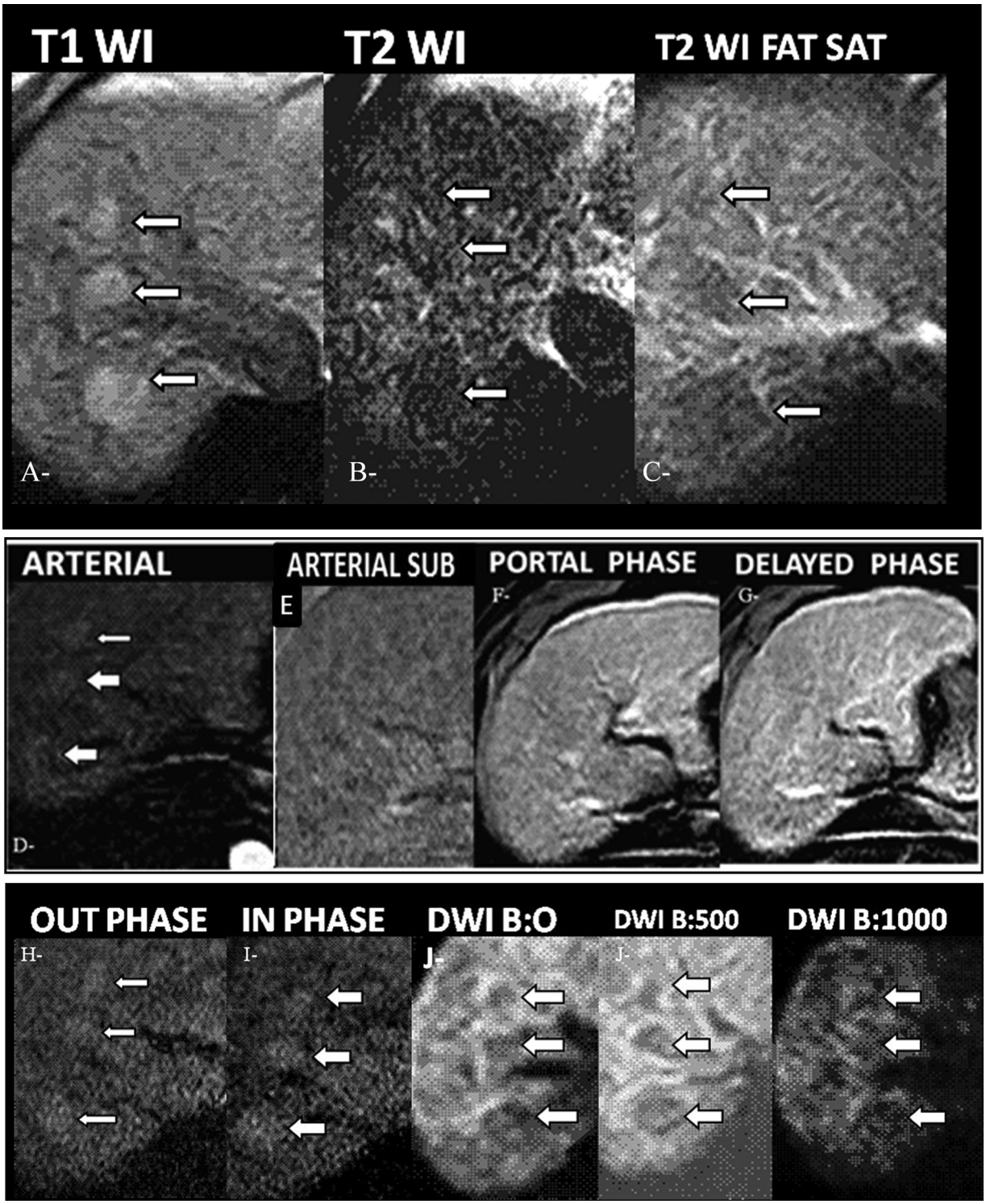

(a–j): A 50-year-old male patient presenting with right hypochondrial pain. US: Cirrhotic liver with three hypoechoic left hepatic lobe focal lesions. Laboratory investigations: α-fetoprotein: 20 ng/ml, alanine transaminase: 25, aspartate aminotransferase: 39. MRI: low-grade dysplastic nodule and was proved by histopathology: Dysplastic nodule with a mild degree of cellular atypia. (a) Axial-unenhanced T1-weighted images: three lesions of high signal intensity in the right hepatic lobe (arrows). (b, c) Axial T2-weighted images (T2WI) and axial T2 fat sat images: They had low signal intensity (arrows). (d, e) Axial-enhanced arterial-phase image: no contrast uptake as seen in the arterial subtraction image (arrows). (f, g) Axial portal and delayed enhanced images: no contrast uptake or washout of the lesions. (h, i) Axial out-phase and in-phase images: They had mild high signal intensity, with no signal drop in the out-phase (no fat content) (arrows). (j) Diffusion-weighted imaging (*b* 0, 500, 1000): They had low signal intensity (arrows).

found in the studies of Jonathon *et al*. [16] and Gaurav *et al*. [11]; both reported that the mosaic pattern is caused by confluent nodules separated by fibrous septa, with necrotic areas, hemorrhage, copper, and fat contents, and it is more prevalent in a large tumor.

Figure 5

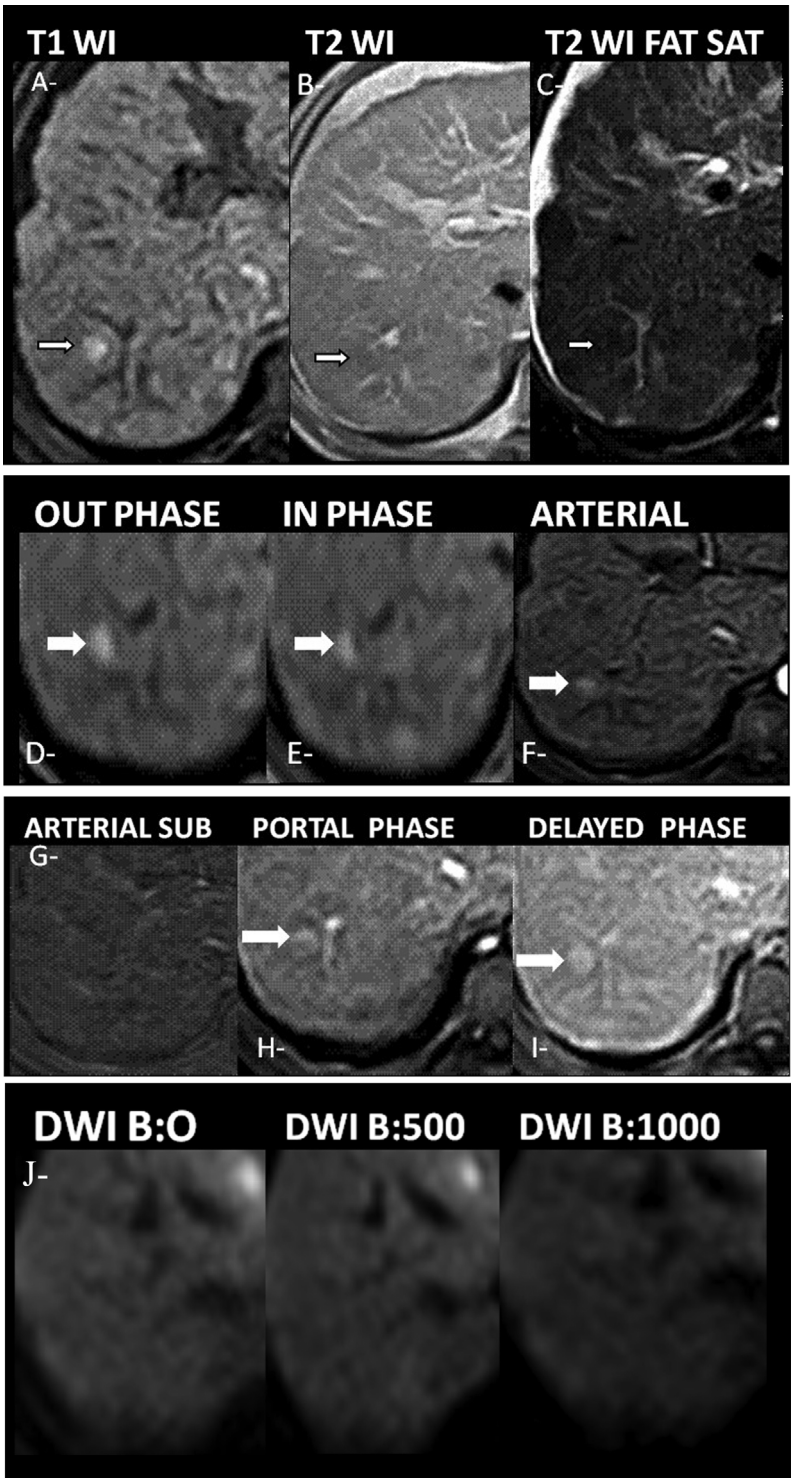

(a–j): A 53-year-old male patient presenting with right hypochondrial pain and yellowish discoloration of the sclera. US: Cirrhotic liver with a hypoechoic right hepatic lobe focal lesion. Laboratory investigations: α-fetoprotein: 35 ng/ml, alanine transaminase: 64, aspartate aminotransferase:43. MRI: High grade dysplastic nodule that was confirmed by histopathology: Dysplastic nodule with a moderate degree of cellular atypia. (a) Axial-unenhanced T1-weighted images: a lesion with high signal intensity in the right hepatic lobe (arrow). (b) Axial T2-weighted images (T2WI): It had mild low signal intensity (arrow). (c) Axial T2 fat sat image: It had low signal intensity (arrow). (d, e) Axial out-phase and in-phase images: It had high signal intensity with no signal drop (arrow). (f, g) Axial-enhanced arterial-phase image: the lesion had a slightly high signal intensity, and this high signal in the arterial phase was related to the high signal intensity of the lesion on T1-weighted images as evident by arterial subtraction image(arrow). (h, i) Axial portal and delayed enhanced images: The lesion showed more brightness (arrow). (j) Diffusion-weighted imaging (*b* 0, 500, 1000): It was isointense to the liver parenchyma.

In our study, all the true-positive group B dysplastic nodules were hyperintense on T1WIs, and hypointense on T2WIs and SPAIR. However, the two falsely diagnosed dysplastic nodules by MRI also

Figure 6

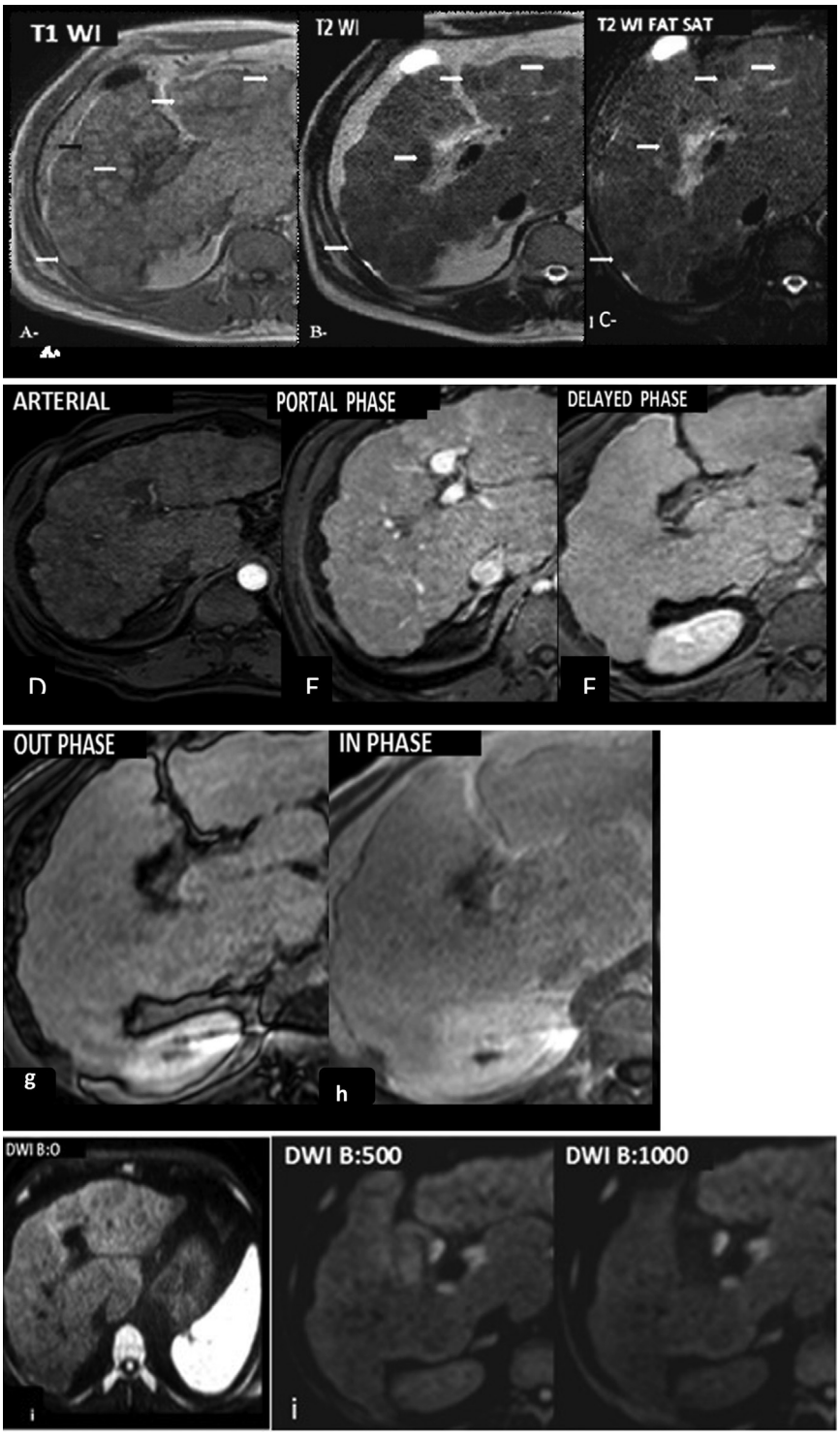

(a–i): A 63-year-old male patient presenting with right hypochondrial pain. US: Cirrhotic liver with multiple iso-echoic hepatic lobe focal lesions. Laboratory investigations: α-fetoprotein: 16 ng/ml, alanine transaminase: 23, aspartate aminotransferase: 25. MRI: multiple regeneration nodules that were confirmed by histopathology. (a) Axial-unenhanced T1-weighted images: multiple lesions of isointense signal similar to the liver parenchyma. (b, c) Axial T2-weighted images (T2WI) and axial T2 fat sat images: The had low signal intensity. (d) Axial-enhanced arterial-phase image: They were isointense. (e, f) Axial portal and delayed enhanced images: They had an isointense signal with no contrast washout. (g, h) Axial out-phase and in-phase images: the lesions were isointense (no fat content). (i) Diffusion-weighted imaging (*b* 0, 500, 1000): isointense lesions.

showed the same signal on these sequences, which is a characteristic feature for dysplastic nodules. The same findings were reported by Gaurav *et al*. [11] and Tatsuyuki *et al*. [20], and they suggested that it could be attributed to deposition of copper, or glycogen, or an increased protein or lipid content.

Figure 7

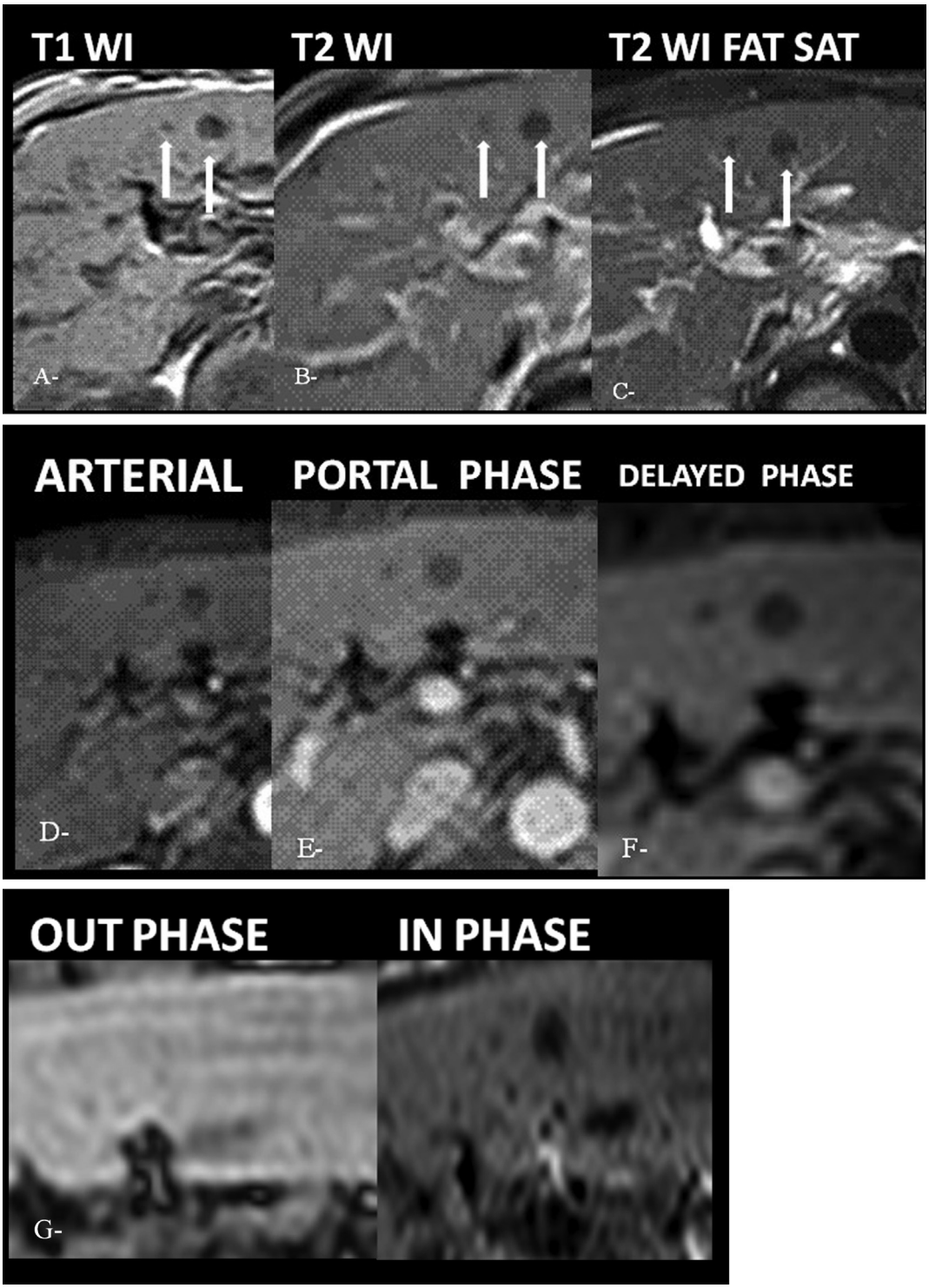

(a–g): A 59-year-old male patient presented with right hypochondrial pain. On US: The liver was cirrhotic, and two hypoechoic left hepatic lobe focal lesions were detected. Laboratory investigations: α-fetoprotein: 15 ng/ml, alanine transaminase: 29, aspartate aminotransferase: 35. Suggested MR diagnosis: siderotic nodules and histopathology: Iron-containing nodules with mild to moderate degree of cellular atypia. (a) Axial unenhanced T1-weighted images showed two lesions of low signal intensity in the left hepatic lobe (arrows). (b, c) Axial T2-weighted images (T2WI) and axial T2 fat sat images showed the lesions to be of low signal intensity (arrows). (d) Axial-enhanced arterial-phase image showed the lesions to be of low signal intensity with no evidence of contrast uptake. (e) Axial portal-enhanced image showed no contrast uptake or washout of the lesions. (f) Axial-delayed enhanced image showed the lesions as still being hypointense. (g) Axial in-phase and out-phase images showed the two lesions to have low signal intensity in the in-phase, whereas in the out-phase, they were hardly seen.

However, Jonathon *et al*. [16] reported that dysplastic nodules may have an inconstant MR appearance, but rarely they appear of high signal intensity on T2WIs and SPAIR.

Figure 8

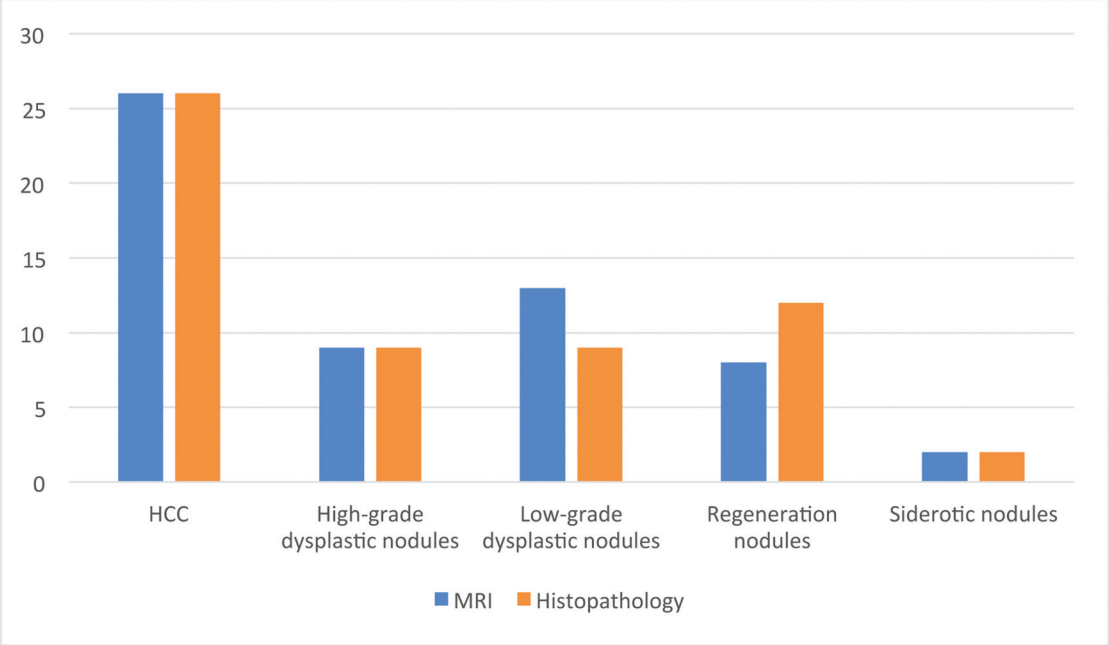

A chart showing the correlation between MR and histopathological results.

This study showed that there was no significant difference between the low-grade and the high-grade dysplastic nodules in their signal intensity pattern on T1WI and T2WIs. However, Robert *et al.* [4] reported that the high-grade dysplastic nodules tend to elicit a slightly hyperintense signal on T2WI. Accordingly, in this state, it may be difficult to differentiate between HCC and the high-grade dysplastic nodule, even on pathology.

In our dynamic MR study, the majority of the high-grade dysplastic nodules showed subtle arterial enhancement, but only one of them showed no arterial contrast uptake. However, all the high-grade dysplastic nodules became more intense than the liver parenchyma in the subsequent portal and delayed phases (Fig. 5). In contrast, all the low-grade dysplastic nodules were isointense to the liver parenchyma in all phases of the dynamic study (Fig. 4).

These findings were also noted by Jonathon *et al.* [16], Tatsuyuki *et al.* [20], and Gaurav *et al.* [11] and Ramalho *et al.* [21], who reported that in terms of the blood supply, the high-grade dysplastic nodules show hypovascularity in the arterial phase with the main portal venous blood supply; thus, they were more enhanced in the portal and delayed phases with no contrast washout. Very few high-grade dysplastic nodules show increased arterial flow with increasing supply from the hepatic artery, and this may overlap with HCC nodules during the process of hepatocarcinogenesis. However, the portal vein supplies low-grade dysplastic nodules and hence, they are isointense to liver parenchyma in all phases of the dynamic enhanced study.

Robert *et al.* [4] and Kreuer *et al.* [22] reported that regenerative nodules show variable signal on T1WIs. On T2WIs, classically, the regenerative nodules were isointense to hypointense, but they almost never elicited a hyperintense signal on T2WI (because of secondary iron deposition). In our study, group C regenerative nodules showed the same findings (Fig. 6). As MR signals of the regeneration nodules were variable, we could not rely on T1WI and T2WIs solely to confirm the diagnosis.

In our dynamic MR study, all of group C regenerative nodules were isointense to the liver parenchyma, with no arterial enhancement or contrast washout owing to the large vascular contribution from the portal vein with minimal supply from the hepatic artery (Fig. 6). These findings were also reported in the study of Seale *et al.* [23].

In our study, the two group D siderotic nodules were characteristically hypointense on T1WIs, T2WIs, and SPAIR sequences. In the dual in-phase and out-phase imaging technique, the siderotic nodules showed a low signal intensity pattern in the in-phase because of its long echo time, whereas in the out-phase, they were

isointense. In our dynamic MR study, the two siderotic nodules were hypointense in all phases, with no imaging features characteristic of their primary nature, whether regeneration or dysplastic nodules (Fig. 7). Robert *et al*. [4] and Krinsky *et al*. [6] reported that no imaging feature (size, number, distribution) is reliable to distinguish the regeneration nodules from dysplastic ones as well as iron containing regeneration nodules from siderotic dysplastic ones.

Accordingly, we generally concluded that DWI was useful in detecting malignant lesions that were restricted or less likely partially restricted in DWIs, whereas the rest of the lesions included in the study (premalignant and benign) showed no restriction.

In our study, the size of the nodules was found to bear relevance to their nature. There were 22 cases of HCC with 26 focal lesions, their size with average diameter of 4.75 cm, 15 cases of dysplastic nodules with 18 focal lesions, with average diameter of 3.03 cm, one case of siderotic nodule with two focal lesions, their size with average diameter of 2.25 cm, two cases of regeneration with 12 focal lesions, their size with average diameter of 1.03 cm, so that as the lesions grow to the larger size, the possibility of malignant lesions is most likely. However, Robert *et al*. [4] reported that lesions with a diameter of less than 2 cm are more likely to be benign and those with a diameter of more than 2 cm are more likely to be malignant. Furthermore, Darnell *et al*. [3], on the basis of AASLD and European Association for the Study of the Liver-European Organization for Research and Treatment of Cancer guidelines, mentioned that if a lesion is more than 10 mm in diameter with characteristic contrast uptake in the arterial phase and washout in the delayed one on dynamic MRI, it is diagnostic of HCC.

We are aware of the limitation of this study because of the relatively small number of patients studied and the use of one kind of contrast medium (Gd-DTPA) to identify the type of nodules. Therefore, further research including large numbers of patients and use of more recent contrast media for nodule detection and characterization would be of great value.

Conclusion

Contrast-enhanced MRI with DWI is sensitive for the early detection of malignant neoplastic hepatic lesions, and for differentiation between the premalignant and the malignant lesions. It offers the advantages of significantly shorter acquisition times, retrospective thin-section or thick-section reconstruction from the same raw data, as well as improved three-dimensional rendering, and high-quality liver imaging with high intrinsic soft-tissue contrast.

Financial support and sponsorship

Nil.

Conflicts of interest

There are no conflicts of interest.

References

1 Popper H. Pathologic aspects of cirrhosis: a review. Am J Pathol 1977; 87:228–264.

2 Hussain SM, Reinhold C, Mitchell DG. Cirrhosis and lesion characterization at MR imaging. Radiographics 2009; 29:1637–1652.

3 Darnell A, Forner A, Rimola J, Reig M, Garcia-Criado A, Ayuso C, Bruix J. Liver imaging reporting and data system with MR imaging: evaluation in nodules 20 mm or smaller detected in cirrhosis at screening US. Radiology 2015; 275:698–707.

4 Hanna RF, Aguirre DA, Kased N, Emery SC, Peterson MR, Sirlin CB. Cirrhosis-associated hepatocellular nodules: correlation of histopathologic and MR imaging features. Radiographics 2008; 28:747–769.

5 Bruix J, Sherman M. Management of hepatocellular carcinoma. Hepatology 2005; 42:1208–1236.

6 Krinsky GA, Lee VS, Nguyen MT, Rofsky NM, Theise ND, Morgan GR, *et al.* Siderotic nodules at MR imaging: regenerative or dysplastic? Radiology 2002; 24:773–776.

7 Van Den Bos IC, Hussain SM, Terkivatan T, Zondervan PE, De Man RA. Stepwise carcinogenesis of hepatocellular carcinoma in the cirrhotic liver: demonstration on serial MR imaging. J Magn Reson Imaging 2006; 24:1071–1080.

8 Maria Loreto Vergara Del R, Manuel Fernandez A, Rondrigo Periera B. DW –MRI characterization of solid liver lesion. Rev Chil Radiol 2010; 16:50.

9 Parikh T, Drew SJ, Lee VS, Wong S, Hetcht EM, Babb JS, Taouli B. Focal liver lesion detection and characterization with diffusion weighted MR imaging. Radiology 2008; 246:812–822.

10 Hosny IA. Diffusion MRI of focal liver lesions. Pak J Radiol 2010; 20:01–07.

11 Khatri G, Merrick L, Miller FH. MR imaging of hepatocellular carcinoma. Magn Reson Imaging Clin N Am 2010; 18:421–450.

12 Krinsky GA, Lee VS, Theise ND, Weinreb JC, Rofsky NM, Diflo T, Teperman LW. Hepatocellular carcinoma and dysplastic nodules in patients with cirrhosis: prospective diagnosis with MR imaging and explantation correlation. Radiology 2001; 219:445–454.

13 Shinmura R, Matsui O, Kobayashi S, Terayama N, Sanada J, Ueda K, *et al.* Cirrhotic nodules: association between MR imaging signal intensity and intranodular blood supply. Radiology 2005; 237:512–519.

14 Van den Bos IC, Hussain SM, Dwarkasing RS, Hop WCJ, Zondervan PE, De Man RA, *et al.* MR imaging of hepatocellular carcinoma: relationship between lesion size and imaging findings, including signal intensity and dynamic enhancement patterns. J Magn Reson Imaging 2007; 26:1548–1555.

15 Watanabe A, Ramalho M, AlObaidy M, Kim HJ, Velloni FG, Semelka RC. Magnetic resonance imaging of the cirrhotic liver: an update. World J Hepatol 2015; 7:468–487.

16 Jonathan M, Willatt, Herok H, Adusumilli S, Marrero JA. MR imaging of hepatocellular carcinoma in the cirrhotic liver: challenges and controversies. Radiology 2008; 247:311–330.

17 Petra GK, Eric J. Diffusion-weighted imaging in the liver. World J Gastroenterol 2010; 16:1567–1576.

18 Wu LM, Xu JR, Lu Q, Hua j, Chen J, Hu J. A pooled analysis of diffusion-weighted imaging in the diagnosis of hepatocellular carcinoma in chronic liver diseases. J Gastroenterol Hepatol 2013; 28:227–234.

19 Demir OI, Obuz F, Sagol O, Dicle O. Contribution of diffusion-weighted MRI to the differential diagnosis of hepatic masses. Diagn Interv Radiol 2007; 13:81–86.

20 Tonan T, Fujimoto K, Qayyum A. Chronic hepatitis and cirrhosis on MR imaging. Magn Reson Imaging Clin N Am 2010; 18:383–402.

21 Ramalho M, Matos AP, AlObaidy M, Velloni FG, Altun E, Semelka RC. Magnetic resonance imaging of the cirrhotic liver: diagnosis of hepatocellular carcinoma and evaluation of response to treatment-part 1. Radiol Bras 2017; 50:38–47.

22 Kreuer S, Elgethun M, Tommack M. Imaging findings of cirrohosis. J Am Osteopath Coll Radiol 2016; 5:5–13.

23 Seale MK, Catalano OA, Saini S, Hahn PF, Sahan DV. Hepatobiliary specific MR contrast agents: role in imaging he liver and biliary tree. Radiographics 2009; 29:1253–1277.